Infrared Observations of the Saturnian System from Voyager 2

Abstract. *During the passage of Voyager 2 through the Saturn system, infrared spectral and radiometric data were obtained for Saturn, Titan, Enceladus, Tethys, Iapetus, and the rings. Combined Voyager 1 and Voyager 2 observations of temperatures in the upper troposphere of Saturn indicate a seasonal asymmetry between the northern and southern hemispheres, with superposed small-scale meridional gradients. Comparison of high spatial resolution data from the two hemispheres poleward of 60° latitude suggests an approximate symmetry in the small-scale structure, consistent with the extension of a symmetric system of zonal jets into the polar regions. Longitudinal variations of 1 to 2 K are observed. Disk-averaged infrared spectra of Titan show little change over the 9-month interval between Voyager encounters. By combining Voyager 2 temperature measurements with ground-based geometric albedo determinations, phase integrals of 0.91 ± 0.13 and 0.89 ± 0.09 were derived for Tethys and Enceladus, respectively. The subsolar point temperature of dark material on Iapetus must exceed 110 K. Temperatures (and infrared optical depths) for the A and C rings and for the Cassini division are 69 ± 1 K (0.40 ± 0.05), 85 ± 1 K (0.10 ± 0.03), and 85 ± 2 K (0.07 ± 0.04), respectively.*

This report summarizes preliminary results obtained by the infrared instrument (IRIS) during the Voyager 2 encounter with Saturn and its satellites. Infrared observations of the Jupiter system from both Voyagers and of the Saturnian system from Voyager 1 were reported previously (*1–7*). Because of a small misalignment of the interferometer, the Voyager 2 IRIS was slightly less sensitive than the Voyager 1 IRIS. At Saturn the noise-equivalent radiance of the Voyager 2 instrument was about four times larger than that of Voyager 1 between 700 and 1000 cm^{-1} and two to three times larger at higher wave numbers; below 500 cm^{-1} both instruments performed nearly the same. Consequently, while Voyager 1 and Voyager 2 spectra yield equally good temperature profiles on Saturn between 50 and 700 mbar, only Voyager 1 spectra permit the derivation of stratospheric temperatures. Furthermore, the responsivity of the Voyager 2 instrument varied slowly as a function of time, and great care was needed to calibrate the spectra in an absolute sense. For that purpose, deep space spectra were accumulated for each period in which the instrument was turned on, and a curve-fitting process was used to find the proper responsivity for each wave number at the time a particular spectrum of an object was taken. This calibration technique has been verified by checking individual deep space spectra for systematic bias.

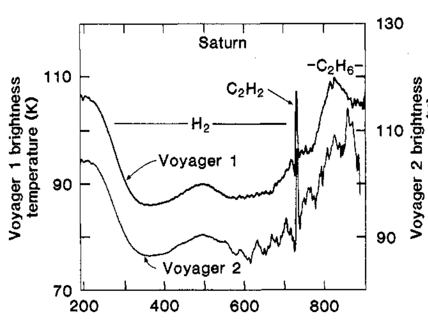

Fig. 1. Comparison of mid-latitude spectra of Saturn obtained by Voyager 1 and Voyager 2. The upper spectrum is an average of 1293 individual Voyager 1 spectra recorded with the field of view centered at 30°N. The lower spectrum is an average of 791 Voyager 2 spectra selected from latitudes between 15° and 50° in both the northern and southern hemispheres.

To take advantage of a different flyby geometry, a number of new observations were planned for the Voyager 2 encounter. However, since most of these observations were to be executed after ring plane crossing, nearly all were lost due to the failure of the spacecraft scan platform. On the inbound trajectory of Voyager 2, observations were obtained of Saturn's northern hemisphere, the disks of Titan, Enceladus, Tethys, and Iapetus, and the illuminated side of the rings. Lost measurements include observations, at high spatial resolution, of Saturn's southern hemisphere and the rings' dark side and eclipses of Tethys, Enceladus, and the ring material. Several days after closest approach some data on the southern hemisphere and the dark side of the rings were recorded, but with relatively low spatial resolution. Nonetheless, useful information was obtained by the Voyager 2 IRIS, and these data complement the conclusions derived from the Voyager 1 spectra.

Saturn. Among the major objectives of the Voyager IRIS investigations of Saturn were measurement of the atmospheric composition, including the He abundance, determination of the planetary heat balance, and inference of the thermal structure of the upper troposphere and stratosphere. Voyager 1 data confirmed the presence of the trace species NH_3, CH_4, PH_3, and C_2H_6; C_3H_4 and C_3H_8 have been tentatively identified. A depletion of atmospheric He on Saturn relative to that on Jupiter is indicated, suggesting that core precipitation of He has occurred to a greater extent on Saturn. Data on atmospheric thermal structure indicate an asymmetry between the northern and southern hemispheres, suggestive of a seasonal response, and thermal wind shears have been calculated and compared with winds derived from Voyager images. The additional data obtained from Voyager 2 contribute to our understanding of these areas.

Figure 1 shows average spectra of Saturn between 200 and 900 cm^{-1}. The Voyager 2 spectrum is an average of 1293 individual spectra recorded between 11 and 3 days before encounter. The IRIS field of view was centered at 30°N. During that period, Saturn's apparent disk increased in angular size from 2.7 to 6.7 times the IRIS field of view. The Voyager 1 spectrum (Fig. 1) is an average of 791 individual spectra recorded 9 months earlier at about 2 days before closest approach, with emission angles of less than 45° and from latitudes between 15° and 50° in both the northern and southern hemispheres. As expected, the Voyager 2 spectrum is very similar to the Voyager 1 spectrum except for the lower signal-to-noise ratio above 500 cm^{-1}. Both spectra show the broad S_0 and S_1 lines of pressure-induced H_2 centered at 354 and 600 cm^{-1}, weak NH_3 lines near 200 cm^{-1} in absorption, and the C_2H_2 line at 729 cm^{-1} in emission.

Investigation of the hemispheric asymmetry of atmospheric structure can be

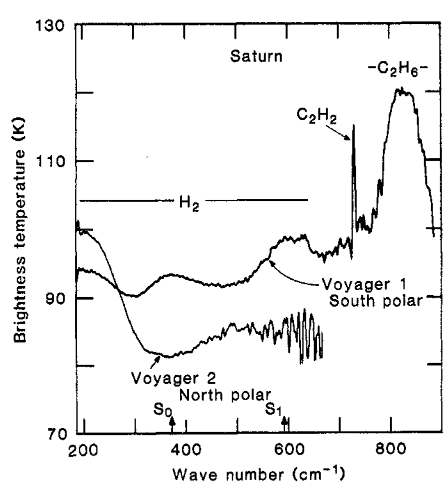

Fig. 2. Comparison of north and south polar spectra of Saturn. The Voyager 2 spectrum is an average of 33 individual spectra acquired with the field of view centered at 78°N. The Voyager 1 spectrum is an average of 38 spectra grouped at 70° and 88°S. The mean emission angle for the north polar spectrum is 59° while that for the south polar spectrum is 76°.

0036-8075/82/0129-0544$01.00/0 Copyright © 1982 AAAS

extended to the polar regions by combining Voyager 2 data from high northern latitudes with Voyager 1 data from high southern latitudes. North and south polar spectra (Fig. 2) display substantially different behavior. The Voyager 2 north polar spectrum is an average of 33 individual spectra recorded approximately 19 hours before closest approach. The field of view was centered at 78°N. Disregarding the noise at the high wave numbers, the north polar spectrum is similar in shape to the mid-latitude spectra shown in Fig. 1, but is on the average about 5 K colder. In contrast, the south polar spectrum from Voyager 1, an average of 38 spectra between 70° and 88°S, shows an inherently different structure. Since the mean emission angle for the north polar spectrum is about 59° while that for the south polar spectrum is 76°, some of the apparent differences are emission angle effects. However, there is a difference in thermal structure between the two polar regions, as shown in Fig. 3. The temperature profiles in the polar regions were obtained by inversion of measured spectra (*8*). The profile for 78°N was retrieved from the Voyager 2 average spectrum, shown in Fig. 2. To obtain the profile at 70°S, a subset of 17 spectra was chosen from the 38 Voyager 1 spectra used for the south polar spectrum average in Fig. 2. This subset was selected to restrict the range in latitude and emission angle.

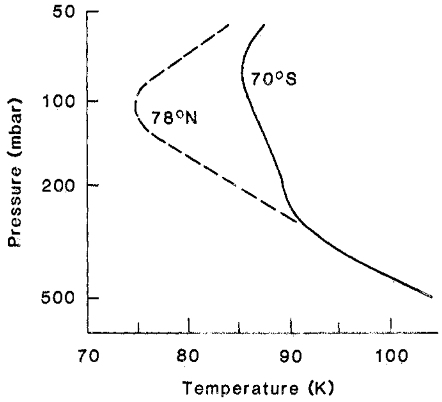

Fig. 3. Temperature profiles for the north and south polar regions of Saturn. The profile for 78°N was derived from the Voyager 2 average spectrum shown in Fig. 2 while that for 70°S was obtained from an average of 17 Voyager 1 spectra.

The tropopause or temperature minimum is approximately 10 K cooler in the north polar region than in the south. Although the profiles are essentially coincident at levels below about 300 mbar, the retrieved temperatures in this region are strongly sensitive to errors in the emission angle at the relatively high air masses associated with the polar spectra, and preliminary pointing information was used in this analysis. Additional uncertainties result from possible contributions to atmospheric opacity by haze and clouds. Therefore, while we can conclude that there is a substantially larger difference in the profiles near the tropopause than at levels below 300 mbar, the precise difference at the deeper levels cannot be specified. Analysis of Voyager 1 data indicates that the general behavior of the profile at 70°S, with a relatively small lapse rate above 300 mbar, persists throughout the southern hemisphere and into the northern hemisphere to approximately 20°N. Farther north the upper tropospheric lapse rate increases, with the shape of the profiles resembling that at 78°N. As pointed out previously (*3*), the relatively cold upper troposphere at high northern latitudes is probably a seasonal effect. Although the northern hemisphere spring equinox occurred in early 1980, the thermal response to solar heating is expected to display a phase lag given by $\tan^{-1}(\Omega_s\tau)$, where $\Omega_s = 2\pi/(\text{Saturnian year})$ and τ is the radiative relaxation time. On the basis of calculations by Gierasch and Goody (*9*), $\Omega_s\tau = 2$ at the 100-mbar level, indicating a lag of about one-sixth of a seasonal cycle, or $\sim$ 5 years. At deeper atmospheric levels, $\Omega_s\tau$ increases, reaching $\sim$ 17 at 700 mbar, implying a lag of one season. However, since the amplitude of the response is approximately inversely proportional to $\Omega_s\tau$, the seasonal variation at the deeper levels is expected to be small, in agreement with the observations.

Voyager 1 data indicated strong latitudinal temperature gradients in the upper troposphere in the northern hemisphere (*3, 4*). Figure 4 shows a composite of temperatures at 150 mbar, obtained by inversion of data from Voyager 1 and Voyager 2. The spatial resolution of the Voyager 1 data, expressed in terms of the projection of the field of view on the planet, was 2° to 5° in latitude; the Voyager 2 spatial resolution was 1° to 2° in latitude. The data from both sets are similar, implying that the meridional temperature structure did not change between the encounters. Previous analysis of Voyager 1 temperatures indicated a good correlation between the calculated thermal wind shear and the winds derived from cloud motion between 30° and 60° latitude (*4*). However, the wind shear

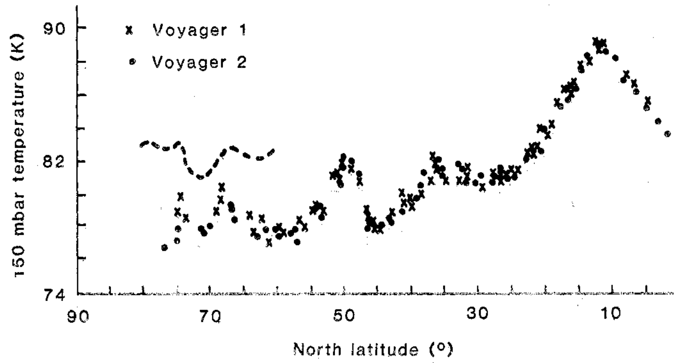

Fig. 4. Temperature as a function of latitude for the 150-mbar level in the atmosphere of Saturn. The dashed line represents Voyager 1 temperatures, displaced downward by 4°, from a high spatial resolution scan at the south pole.

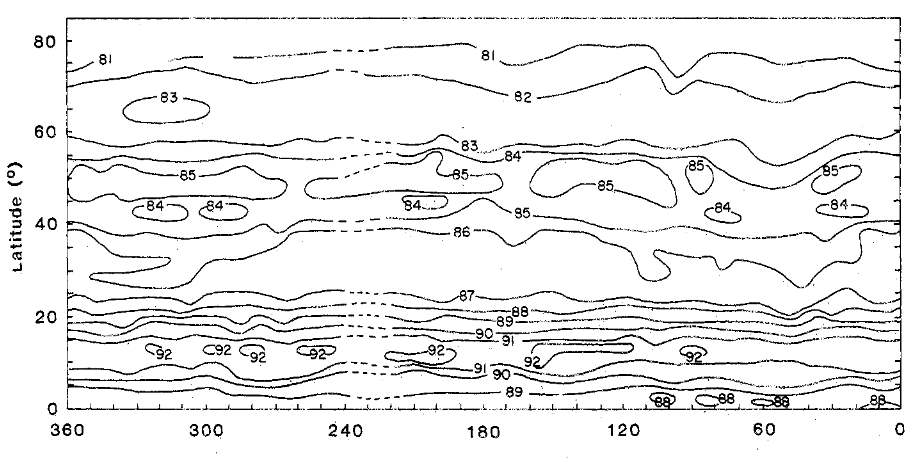

Fig. 5. Map of Saturn brightness temperatures averaged within the spectral interval 330 to 400 cm^{-1}. Emission in this interval originates from a region centered near 150 mbar. The data were acquired with a spatial resolution corresponding to about 8° in latitude or longitude at low latitudes. The dashed contours are interpolations over longitudes not covered during the mapping sequence.

calculated from the strong temperature gradient observed by Voyager 1 between 12° and 23°N, and confirmed by Voyager 2, is not correlated with winds derived from images in this region. The composite data set (Fig. 4) indicates the presence of additional gradients between 60° and 80°N which suggest continuation of the system of alternating eastward and westward jets into the high latitude region. These observations appear to be consistent with cloud-top winds obtained from Voyager 2 images, which also show a continuation of the jet system into the polar regions (*10*). In addition, temperatures obtained between 60°S and the south pole by Voyager 1 (*3*) show small-scale latitudinal gradients similar to those at high northern latitudes (Fig. 4). This indicates an approximate symmetry in the latitudinal dependence of the thermal wind shear, at least poleward of 60° latitude. Unfortunately, few high spatial resolution data were obtained by Voyager 1 or Voyager 2 between the equator and 60°S.

Although infrared observations of Jupiter by Voyager 1 and Voyager 2 indicated significant departure from zonal symmetry in the atmospheric temperature field (*1*), Voyager 1 observations suggested that longitudinal structure in Saturn's atmospheric temperature was much less pronounced (*3*). To determine the longitudinal dependence of the atmospheric thermal structure, data from a north-south mapping sequence have been analyzed. Figure 5 shows brightness temperatures averaged over the spectral interval 330 to 400 cm^{-1} and corresponding to temperatures in an atmospheric layer centered near 150 mbar. Observations were made at intervals of 5° in latitude and longitude, with a projected field of view of 8° in latitude and longitude at low and mid-latitudes. Although this resolution is not as good as that of the data in Fig. 4, the latitudinal gradients observed in the high-resolution data can be seen here, but with reduced magnitudes. A small longitudinal temperature structure, with amplitudes of 1 to 2 K, can also be discerned. Similar Voyager 1 mapping sequences with lower spatial resolution exhibit similar structure in latitude and longitude. To examine the longitudinal structure more quantitatively, brightness temperatures from all longitudes were plotted as a function of latitude (Fig. 6). The largest longitudinal variations are in the regions 35° to 42°N, 50° to 57°N, and poleward of 65°N. The first two regions correspond to relatively weak retrograde jets. Images of these regions [figures 4 and 5 in (*11*)] suggest the presence of convective activity morphologically different from that in other regions of the planet.

The acquisition of IRIS spectra at the Voyager 2 radio occultation points, for which the observational geometry was more favorable than in the case of Voyager 1, will contribute to a refinement of the He abundance determination. Also, the extension of coverage to high northern latitudes will aid in the study of the heat balance of Saturn. However, substantial analytical efforts are required in both areas before final results can be obtained.

Titan. The close approach of Voyager 1 to Titan permitted the recording of infrared spectra at high spatial resolution. IRIS has established the presence of 11 atmospheric constituents, including organic compounds and molecules containing hydrogen, nitrogen, and carbon in several combinations. It also revealed the existence of an atmospheric window at about 540 cm^{-1} (*3, 6*).

Voyager 2 could not obtain spectra at high spatial resolution because of the relatively large distance between the spacecraft and Titan. A total of 118 usable spectra were obtained in a period of 16 hours when the angular diameter of Titan ranged from 0.4° to 0.5°, comfortably exceeding the 0.25° IRIS field of view. The average of these spectra is shown in Fig. 7 with an average of 82 Voyager 1 spectra recorded 9 months earlier at the same distances from Titan.

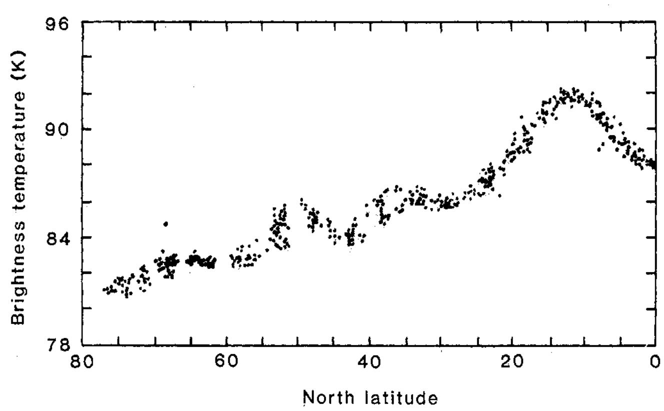

Fig. 6. Envelope of brightness temperatures, averaged within the spectral interval 330 to 400 cm^{-1}. Data are from the north-south mapping sequence shown in Fig. 5. Emission in this interval originates from a region centered near 150 mbar. The width of the envelope indicates the variation of temperature with longitude.

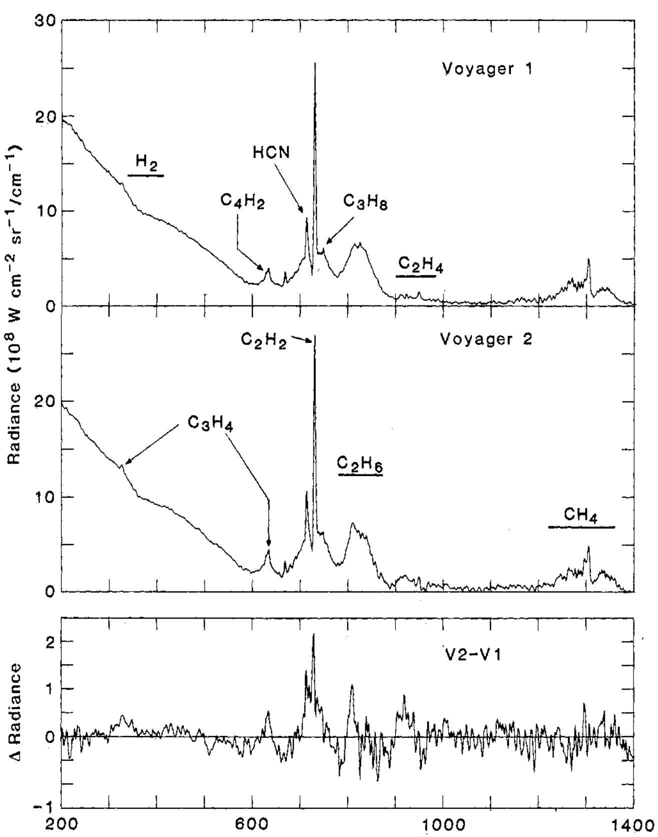

Fig. 7. Averages of 82 Voyager 1 and 118 Voyager 2 spectra of Titan and their difference spectrum (Voyager 2 minus Voyager 1). The difference spectrum is in the same units as the individual spectra. The hydrocarbons are seen in emission in the stratosphere, while molecular hydrogen is seen in absorption in the troposphere.

Both spectra show the S_0 absorption line of H_2 and emission features of CH_4, C_2H_2, C_2H_6, C_3H_4, C_4H_2, HCN, C_2H_4, and C_3H_8; the last two are not as sharply defined in the Voyager 2 spectrum owing to its intrinsically higher noise level at the corresponding wave numbers. In other respects the spectra are quite similar. They are almost identical in the regions around 540, 200, and 1304 cm^{-1}, which correspond to emissions from the surface, the tropopause, and the stratosphere, respectively (*5, 6*). This indicates that any differences in other spectral regions are not likely to be caused by atmospheric or surface temperature differences. Although the differences may not be significant, the C_3H_4 band at 327 cm^{-1}, the blend of C_3H_4 and C_2H_2 at 630 cm^{-1}, and the HCN-C_2H_2 continuum across the region from 710 to 730 cm^{-1} are slightly enhanced in the Voyager 2 spectrum, implying there may have been a slight overall opacity or composition change over the 9-month interval between encounters. The differences might also be symptomatic of slightly different effective emission angles and fields of view, although considerable effort was made to ensure comparable data sets. Differences over the spectral region 750 to 1000 cm^{-1} are not regarded as significant because of the relatively higher Voyager 2 noise-equivalent radiance in this region.

Tethys. Three observations were obtained at phase angles between 19° and 14°, with the satellite filling between 12 and 20 percent of the IRIS field of view. After correcting for the filling fraction, a 200-cm^{-1} disk brightness temperature of 87 ± 4 K is obtained at a mean phase angle of 16°; the error mainly represents a limit on systematic effects due to pointing uncertainties and to position-dependent variations in sensitivity across the instrument's field of view.

To derive a bolometric Bond albedo and phase integral from this datum, models of the surface temperature distribution and local phase function are required (*12*). A simple model for an airless object is $T(\theta) = T_{ss} \cos^{1/n} \theta$, where T_{ss} and θ are subsolar point temperature and zenith angle of the sun, respectively. For a nonrotating Lambert sphere $n = 4$. For the moon $n \simeq 6$ (*13*). A fit to Voyager data for Rhea (*3*) gives $n \simeq 7$. We adopt $n = 7 \pm 1$ for Tethys. With this temperature distribution integrated over the disk and corrected for the 16° phase angle, $T_{ss} = 93 \pm 4$ K is obtained. The bolometric Bond albedo is then found to be

$$A = 1 - R^2\, T_{ss}^{\,4}/T_0^{\,4} = 0.73 \pm 0.05$$

Table 1. Normal infrared optical depths and brightness temperatures in Saturn's rings. The emission angle of the observations was ~ 67°.

Source	τ_{ring}	T_{ring} (K)
A ring	0.40 ± 0.05	69 ± 1
Cassini division	0.07 ± 0.04	85 ± 2
Outer B ring	0.8 ± 0.2	68 ± 1
Outer C ring	0.10 ± 0.03	85 ± 1

where R, the distance between Saturn and the sun, is 9.601 AU, and T_0, allowing for peaking of infrared flux at small phase angles, is 401 ± 6 K. With the geometric albedo $p = 0.8 \pm 0.1$, as determined from ground-based measurements and corrected for the recently refined satellite radius (*11*), the phase integral of Tethys becomes $q = A/p = 0.91 \pm 0.13$, in agreement with values for other icy bodies (*13, 14*).

Enceladus. Four observations were obtained at phase angles between 39° and 36°, with the satellite filling between 13 and 32 percent of the instrument's field of view. These yield a 200-cm^{-1} disk brightness temperature of 67 ± 2 K at a mean phase angle of 37°. Following the analysis for Tethys, a subsolar point temperature for Enceladus of 75 ± 3 K is obtained. This includes a 1 K additive correction to account for peaking of the infrared radiation in the sunward direction, as occurs on Rhea (*3*). The bolometric Bond albedo and phase integral for the satellite are then 0.89 ± 0.02 and 0.89 ± 0.09, respectively, where the geometric albedo $p = 1.0 \pm 0.1$ as determined from combined ground-based and Voyager observations (*11*). An additional observation of Enceladus at a phase angle of 42°, in which the projected diameter of the IRIS field of view was 85 percent of the satellite's diameter, yields similar results. Again, these are in agreement with values for other icy satellites.

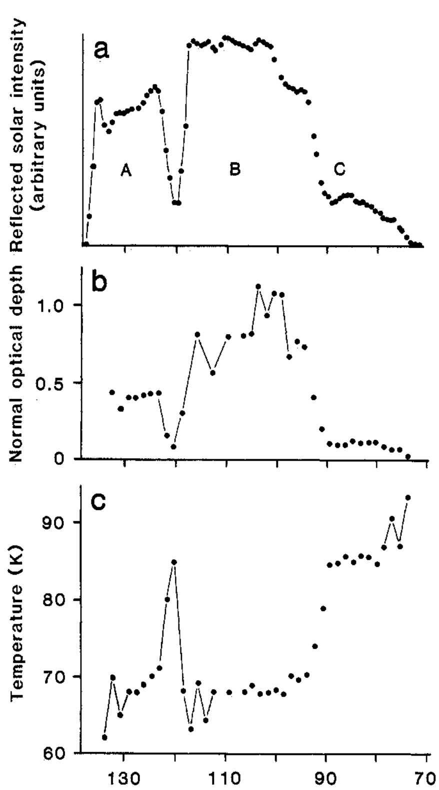

Fig. 8. Results from radial ring scan of the illuminated side of Saturn's rings. (a) Reflected solar intensity, as observed by the IRIS radiometer. (b) Normal infrared optical depths, as determined by using thermal spectra obtained simultaneously with the radiometer data. The radiometer and infrared optical axes are bore-sighted. A homogeneous, nonscattering slab model was used for the analysis. No correction for phase angle (46°) or mutual shadowing of the ring particles was made. (c) Ring temperatures derived by using the slab model.

Iapetus. Observations were obtained at phase angles of 48°, 67°, and 80°, with the satellite filling approximately 10 percent of the instrument's field of view. A subsolar point temperature for the dark component in excess of 110 K is indicated, which is consistent with the low albedo of this material (*10*). Further analysis requires incorporation of the albedo distribution across the disk at the times of the observations.

Rings. Approximately 9 hours before closest approach to Saturn a scan was made from outside the A ring to within the C ring (Fig. 8). The width of the IRIS field of view projected on the ring plane was about 3500 km, or approximately the width of the Cassini division. The intensity scan in reflected sunlight (Fig. 8a) shows radial structure virtually identical to that in a solar transmission observation by IRIS from Voyager 1; in that scan, which extended from the middle of the B ring to well beyond the F ring [see figure 12 in (*3*)], the projected solar disk diameter was also approximately equal to the width of the Cassini division.

The ring particle temperatures and the mean ring optical depth in the infrared can be estimated from the thermal spectra obtained simultaneously with the reflected solar radiation data. A simple model considers the ring as a thin, homogeneous, nonscattering slab that radiates as a blackbody. The observed thermal emission as a function of wave number, I_ν, will then be related to the blackbody emission of the material, $B_\nu(T_{ring})$, by

$$I_\nu = (1 - e^{-\tau_{ring}/\cos\theta}) B_\nu(T_{ring})$$

where T_{ring} and τ_{ring} are the blackbody temperature and normal infrared optical depth of the ring material and θ is the emission angle measured from the ring plane normal.

From averages of pairs of spectra in the ring scan, intensities at 200 and 400 cm^{-1} were used to derive normal infrared optical depths and ring temperatures (Fig. 8, b and c). If the system is optically thick the optical depth is poorly determined because of sensitivity to noise, as is evident for the B ring (Fig. 8b). The results are summarized in Table 1. The results for the C ring are in agreement with those from Pioneer (*15*) and are identical to those derived from Voyager 1 data by applying the above model to observed variations of infrared intensity with emission angle (*3*). No similar calculations were made for the A and B rings with Voyager 1 data. The normal optical depths of the A and C rings and of the Cassini division are in agreement with values at similar spatial resolution at shorter wavelengths (*11, 15, 16*). Discrepancies may exist with longer wavelength observations (*15, 17*). The sensitivity of the simple model to noise for an optically thick system and the neglect of phase angle corrections and of mutual shadowing among ring particles make detailed quantitative comparison of these results with other data premature.

R. HANEL
B. CONRATH
F. M. FLASAR
V. KUNDE
W. MAGUIRE
J. PEARL
J. PIRRAGLIA
R. SAMUELSON
NASA Goddard Space Flight Center, Greenbelt, Maryland 20771
D. CRUIKSHANK
University of Hawaii, Honolulu 96822
D. GAUTIER
Paris Observatory, Meudon, France
P. GIERASCH
Cornell University, Ithaca, New York 14853
L. HORN
Jet Propulsion Laboratory, Pasadena, California 91109
C. PONNAMPERUMA
University of Maryland, College Park 20742

References and Notes

1. R. A. Hanel *et al.*, *Science* **206**, 952 (1979).
2. R. A. Hanel *et al.*, *ibid.* **204**, 972 (1979); J. Pearl, R. Hanel, V. Kunde, W. Maguire, K. Fox, S. Gupta, C. Ponnamperuma, F. Raulin, *Nature (London)* **280**, 755 (1979); R. A. Hanel, B. J. Conrath, L. W. Herath, V. G. Kunde, J. A. Pirraglia, *J. Geophys. Res.* **86**, A10, 8705 (1981); D. Gautier, B. Conrath, M. Flasar, R. Hanel, V. Kunde, *ibid.*, p. 8713; B. J. Conrath, F. M. Flasar, J. A. Pirraglia, P. J. Gierasch, G. E. Hunt, *ibid.*, p. 8769; F. M. Flasar, B. J. Conrath, J. A. Pirraglia, P. C. Clark, R. G. French, P. J. Gierasch, *ibid.*, p. 8759; G. Hunt, B. Conrath, J. Pirraglia, *ibid.*, p. 8777; A. Marten *et al.*, *Icarus* **46** (1981).
3. R. A. Hanel *et al.*, *Science* **212**, 192 (1981).
4. J. A. Pirraglia, B. J. Conrath, M. D. Allison, P. J. Gierasch, *Nature (London)* **292**, 677 (1981).
5. F. M. Flasar, R. E. Samuelson, B. J. Conrath, *ibid.*, p. 693.
6. W. C. Maguire, R. A. Hanel, D. E. Jennings, V. G. Kunde, R. E. Samuelson, *ibid.*, p. 683; V. G. Kunde, A. C. Aikin, R. A. Hanel, D. E. Jennings, W. C. Maguire, R. E. Samuelson, *ibid.*, p. 686; R. E. Samuelson, R. A. Hanel, V. G. Kunde, W. C. Maguire, *ibid.*, p. 688.
7. R. Hanel, D. Crosby, L. Herath, D. Vanous, D. Collins, H. Creswick, C. Harris, M. Rhodes, *Appl. Opt.* **19**, 1391 (1980).
8. B. J. Conrath and D. Gautier, in *Remote Sensing of Atmospheres and Oceans*, A. Deepak, Ed. (Academic Press, New York, 1980), p. 611.
9. P. J. Gierasch and R. M. Goody, *J. Atmos. Sci.* **26**, 979 (1969).
10. B. A. Smith *et al.*, *Science* **215**, 504 (1982).
11. B. A. Smith *et al.*, *ibid.* **212**, 163 (1981).
12. D. P. Cruikshank and T. J. Jones, *Icarus* **31**, 427 (1977).
13. J. M. Saari, R. W. Shorthill, D. F. Winter, *Moon* **5**, 179 (1972).
14. D. Morrison, in *Planetary Satellites*, J. A. Burns, Ed. (Univ. of Arizona Press, Tucson, 1977), p. 269.
15. L. Froidevaux and A. P. Ingersoll, *J. Geophys. Res.* **85**, 5929 (1980).
16. L. W. Esposito, J. P. Dilley, J. W. Fountain, *ibid.*, p. 5948; B. R. Sandel *et al.*, *Science* **215**, 548 (1982).
17. G. L. Tyler, V. R. Eshleman, J. D. Anderson, G. S. Levy, G. G. Lindal, G. E. Wood, T. A. Croft, *ibid.* **212**, 201 (1981).
18. We thank L. Mayo, J. Frost, J. Tingley, and J. Hornstein for their support in data processing and programming.

10 November 1981

Extreme Ultraviolet Observations from the Voyager 2 Encounter with Saturn

Abstract. *Combined analysis of helium (584 angstroms) airglow and the atmospheric occultations of the star δ Scorpii imply a vertical mixing parameter in Saturn's upper atmosphere of* K *(eddy diffusion coefficient)* $\sim 8 \times 10^7$ *square centimeters per second, an order of magnitude more vigorous than mixing in Jupiter's upper atmosphere. Atmospheric* H_2 *band absorption of starlight yields a preliminary temperature of 400 K in the exosphere and a temperature near the homopause of* ~ 200 *K. The energy source for the mid-latitude* H_2 *band emission still remains a puzzle. Certain auroral emissions can be fully explained in terms of electron impact on* H_2*, and auroral morphology suggests a link between the aurora and the Saturn kilometric radiation. Absolute optical depths have been determined for the entire C ring and parts of the A and B rings. A new eccentric ringlet has been detected in the C ring. The extreme ultraviolet reflectance of the rings is fairly uniform at 3.5 to 5 percent. Collisions may control the distribution of H in Titan's H torus, which has a total vertical extent of* ~ 14 *Saturn radii normal to the orbit plane.*

Saturn's atmosphere. The H, H_2, and He of Saturn's upper atmosphere emit characteristic radiation in the extreme ultraviolet (EUV) wavelengths. Although resonance scattering of the strong solar lines at H Lyman α and He 584 Å accounts for much of the equatorial and mid-latitude emission at those wavelengths, mid-latitude emissions originating from electron-excited H and H_2 were also observed.

The brightness of the He 584 Å line increased from 2.2 ± 0.3 rayleigh (R) during the Voyager 1 encounter (*1*) to 4.2 ± 0.5 R during the Voyager 2 encounter, indicating that important changes have occurred in the upper atmosphere (*2*). Models of the He 584 Å dayglow (*3*) require either a decrease of the temperature (*T*) in the scattering region or an increase in the eddy diffusion coefficient (*K*) (*4*) to account for the observed change. The H Lyα brightness should be strongly anticorrelated with the He 584 Å brightness (*3*), whereas only a slight decrease from 3.3 kR (Voyager 1) to 3.0 kR (Voyager 2) was observed.

In principle it is possible to derive a value of *K* from the H Lyα brightness (*5*) and remove the *T*-*K* ambiguity, but in practice this procedure leads to uncertain results because H Lyα can be excited by mechanisms other than resonance scattering of the solar line, and H can be supplied by processes other than dissociation of molecules by solar radiation (*6*). Elsewhere (*7*) we combine information obtained from a stellar occultation with the He model to derive a *T*, *K* pair consistent with both sets of data. The values are $K \sim 8 \times 10^7$ cm^2 sec^{-1} and $T = 170$ K near the homopause. The large H Lyα brightness of the planet can probably be reconciled with the large value of *K*, given the possibility of additional excitation mechanisms and additional sources of H. The equatorial and mid-latitude H_2 band intensity was the same at both encounters.

Measurements of H_2 band emissions from Saturn's mid-latitudes have empha-

0036-8075/82/0129-0548$01.00/0 Copyright © 1982 AAAS